Groundwork for GNSS integrity monitoring in urban road applications. The road user charging case

Daniel Salós, Anaïs Martineau, Christophe Macabiau, Damien Kubrak, Bernard Bonhoure

Groundwork for GNSS Integrity Monitoring in Urban Road Applications. The Road User Charging Case.

D. Salós, *TéSA*; A. Martineau, C. Macabiau, *ENAC*; D. Kubrak, *Thales Alenia Space*; B. Bonhoure, CNES

BIOGRAPHIES

Daniel Salós graduated as a telecommunication engineer in 2006 from the University of Saragossa, Spain. Since 2008 he is a Ph.D. student at the signal processing laboratory of the ENAC in Toulouse, France, working on GNSS integrity monitoring techniques for urban environments.

Anaïs Martineau graduated in 2005 as an electronics engineer from the Ecole Nationale de l'Aviation Civile (ENAC) in Toulouse, France. Since 2005, she has been working at the signal processing lab of the ENAC where she carries out research on integrity monitoring techniques. She received her Ph.D. in 2008 from the University of Toulouse.

Christophe Macabiau graduated as an electronics engineer in 1992 from the ENAC in Toulouse, France. Since 1994, he has been working on the application of satellite navigation techniques to civil aviation. He received his Ph.D. in 1997 and has been in charge of the signal processing lab of the ENAC since 2000. His research now also applies to vehicular, pedestrian and space applications, and includes advanced GNSS signal processing techniques for acquisition, tracking, interference and multipath mitigation, GNSS integrity, as well as integrated GNSS inertial systems and indoor GNSS techniques.

Bernard Bonhoure graduated as an aeronautic engineer from ENSICA in Toulouse (ISAE). He joined CNES in 1989, he has worked on several successful space programmes such as TOPEX/POSEIDON, SPOT, ENVISAT, JASON. As a navigation system expert, he is now involved in many activities linked to GNSS satellite positioning and performances.

Damien Kubrak graduated in 2002 as an electronics engineer from ENAC, Toulouse, France. He received his Ph.D. in 2007 from ENST Paris, France. Since 2006, he is working at Thales Alenia Space, Toulouse, France, where he is involved in land vehicle navigation, GNSS signal processing and hybridization for seamless positioning, assisted GNSS and mobile phones performance assessment.

ABSTRACT

GNSS-based Road User Charging (RUC) systems have recently attracted special attention because of their flexibility and reduced roadside infrastructure. For instance, German and Slovak motorways already perform truck toll collection by means of GPS receivers installed on the vehicles. Road toll belongs to the so-called liability critical applications, which are characterized by the fact that they must use trustful positioning data in order to control the navigation errors and their negative legal or economical consequences. Consequently, integrity monitoring of GNSS signals plays a key role in such systems. Nevertheless, the design of GNSS integrity algorithms like RAIM requires a deep knowledge of the characteristics of the application, the received signals and the environment effects on them. This paper analyzes and provides the required parameters to develop RAIM algorithms for road tolling applications in urban and rural environments.

1. INTRODUCTION

Road User Charging (RUC) systems are mechanisms through which vehicles pay for travelling through a determinate area or portion of road, like motorway tolls as example. They may be implemented in different ways: tollbooths, gates equipped with number plate recognition, dedicated short-range communications (DSRC), GNSS etc. Among all these possible technologies, schemes based on GNSS are particularly interesting because they provide free-flow (pay-as-you-drive) systems with a very flexible design and a reduced quantity of roadside infrastructures, which also reduces the required investment per kilometer of charged road. These reasons, together with the possibility of interoperability of RUC systems deployed in different countries, have led the European Union to recommend the application of satellite positioning and mobile communications technologies in the new electronic toll systems [1].

GNSS-based electronic tolling systems (ETS) are already becoming a reality. As of 2010, two truck tolling systems based on GPS are already deployed in Germany (where the system is known as LKM Maut) [2] and Slovakia [3]. Their coverage includes the motorway network and some additional roads. Moreover, GNSS technology is being considered in other national RUC projects like the different payment for mobility (ABvM) in the Netherlands [4] or the heavy goods vehicle eco-tax in France [5].

Liability-critical GNSS applications are defined by the fact that an excessive and uncontrolled error in the estimated position may have negative legal or economical consequences. GNSS-based RUC systems are liability-critical because erroneous user localization may cause incorrect tolling bills, which in turn may cause loss of revenue in the case of undercharging (the amount of money charged to the user is lower than it should), or user claims in the case of overcharging (the amount of money charged to the user is higher than it should). In any case, incorrect invoices damage the system's credibility. Thus, bill errors must be monitored and limited according to the application's required performances, what implicitly also sets the bounds of the positioning errors. For this reason, GNSS integrity monitoring is a key element of road toll systems that assures the position errors are below the specified limits, detecting unacceptably large errors and indicating when it is not possible to obtain a navigation solution within the integrity requirements.

GNSS integrity monitoring algorithms cannot be designed without a detailed characterization of the required performances and of the expected positioning errors. In addition, RUC systems should be able to work in urban and suburban environments, where GNSS integrity monitoring might be a challenging task due to the reduced satellite visibility and error sources like multipath. The aim of this paper is to provide the models and parameters needed in the design of integrity monitoring algorithms, in particular RAIM (Receiver Autonomous Integrity Monitoring), for road tolling applications in urban environments.

The paper is structured in the following manner. Section 2 presents the concepts of geo-fencing and road segmentation and section 3 defines the parameters that describe GNSS integrity and RAIM algorithms. The application's required performances and their relation with the GNSS integrity requirements are established in section 4. A study of the satellite visibility in urban environment is given in section 5. The nominal errors are modeled in section 6 and their correlation time is characterized in section 7. Finally, threat model is studied in section 8, where the critical bias is calculated.

2. GEO-FENCING: ROAD SEGMENTATION

RUC systems may have different charging criteria depending on their application. For instance, road and highway tolls are usually determined according to the distance circulated by the user, whereas city center perimeters are likely to be charged as a fixed price for entering the area or as a function of the time spent inside.

This work focuses on road tolling rather than on congestion area pricing, so a distance-based charging approach is chosen. This is achieved using geo-fencing techniques that split the road network into segments defined by virtual perimeters. The areas contained in these virtual perimeters are known as geo-objects and constitute the basic charging units. If road segments are defined as road portions between intersections, with only one entrance and one exit, their associated charge can be proportional to the distance travelled by the user. The segment's price function is flexible and may depend not only on its length but also on the vehicle type, the time of the day, the geographical area, etc. Both existing GNSS-based ETS for trucks in Germany and Slovakia have this kind of road segmentation. In general, geo-fencing is a versatile technique that can also be used in other RUC systems like city center perimeter charging.

Once the geo-objects have been defined, the toll system's user detection mechanism decides in which ones a vehicle has been. This decision is based on the position and integrity monitoring information calculated by the GNSS receiver installed at the user's vehicle. The final bill is the addition of the charges associated to each road segment where the user has been detected in.

In general, the segment's length has an impact on the performance of the user detection process, also known as geo-object recognition. The longer a road segment is, the longer it takes a vehicle to travel through it and the higher is the probability of having adequate conditions (satellite visibility and geometry) that allow reliable GNSS positioning. As an example, the average segment's length in the LKM Maut system is 4.6 km (Figure 1). Nevertheless, it mainly covers the motorway network, so the segment's length in other type of roads with more frequent intersections is expected to be shorter.

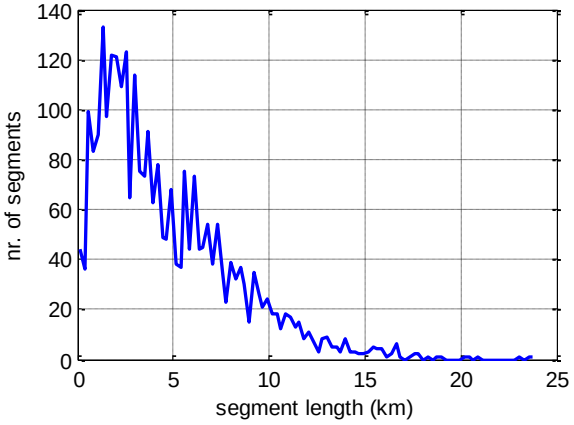

Figure 1. Histogram of segment length in the LKM Maut system.

3. CONCEPTS OF GNSS INTEGRITY CONTROL FOR ROAD TOLLING

As a liability critical application, RUC's user detection mechanisms rely on the integrity associated to the estimated position, which is defined as a measure of the trust on the correctness of the navigation information furnished by the GNSS receiver. Thus, GNSS integrity monitoring mechanisms are a fundamental element of a RUC system.

This section introduces various notions and definitions related with GNSS integrity monitoring. As GNSS integrity has been originally developed in the frame of civil aviation, most of the parameters presented here are the adaptation to road applications of those defined in civil aviation standards [6], [7].

A. Types of GNSS integrity monitoring systems

GNSS integrity can be monitored with different systems. In the case of GPS, integrity must be monitored by augmentation systems like GBAS or SBAS because standalone GPS does not provide integrity services. On the other hand, Galileo projects to have its own integrity monitoring network and will provide a safety of life (SoL) service. Nevertheless, all these integrity control systems have been conceived to meet the civil aviation requirements, which may be different from those ones of road applications. In addition, they rely on ground base stations, which makes them incapable to handle local errors caused by the user's immediate environment such as multipath.

Although SBAS integrity alerts are conceived for civil aviation applications, SBAS differential corrections and residual error models of certain pseudorange errors like ionospheric delay or satellite clock and orbit inaccuracies are still applicable to road applications.

This paper addresses the receiver autonomous integrity monitoring (RAIM), which are algorithms performed at the GNSS receiver itself that only use ranging measurements. RAIM is based on redundancy, that is, it needs to track a higher number of ranging sources than the minimum required to calculate the position only. Because RAIM works only with measured ranges, it presents some interesting properties like the capability of dealing with real local errors. RAIM can be used with any GNSS, including combinations of them, and applications with different integrity requirements just need to install at the receiver an appropriate algorithm designed to meet them.

B. Definition of GNSS integrity requirements

Integrity is defined as a measure of the trust that can be placed in the correctness of the information supplied by the total system, including the ability to provide timely and valid alerts when the system must not be used [7].

The GNSS integrity requirements of road applications that use 2D positioning are defined by the three following parameters [6]:

- **Integrity risk (P_{int})**, is the required maximum probability that a GNSS receiver equipped with integrity monitoring algorithms provides a position failure without alerting the user within the maximum time-to-alert.
- **Time-to-alert (TTA)** is the maximum allowable elapsed time from the onset of a positioning failure until the equipment annunciates the alert.
- **Horizontal Alert Limit (HAL)**, is the radius of a circle with its center at the true position, that describes the region that is required to contain the estimated horizontal position with the required probability.

In the case of applications with 3D navigation and integrity requirements in the vertical direction, a vertical alert limit (VAL) has to be defined.

Position failures are excessively large position errors that the application (the geo-object recognition algorithm in the case of RUC) should not use. They are defined to occur whenever the difference between the true position and the estimated position exceeds the HAL (Figure 2):

$$\left| X_H - \hat{X}_H \right| > HAL \Rightarrow X_{failure} \quad (1)$$

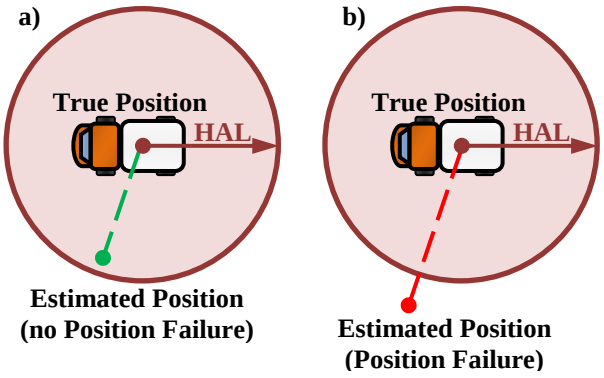

Figure 2. Upper view of a truck with examples of a) valid estimated position, b) position failure.

In other words, the HAL defines the maximum allowable horizontal position error. In road tolling the HAL can be determined as half of the minimum separation between roads, which is the maximum position error of a vehicle situated at one side of the road that still allows to detect its presence on the correct road. A constant HAL is taken in order to keep a simple detection algorithm, although larger HAL are possible for vehicles circulating in the center of the road or at places with larger separation between roads. Then, geo-objects are finally defined by the road sections between crossings plus the HAL around

the road limits. The value of HAL depends on the given road network to be charged.

Civil aviation are real time operations where the TTA represents the maximum time interval the pilot may handle a position failure. Road tolling may perform geo-object recognition off-line, so the TTA cannot be applied in the same way. Furthermore, the design of snapshot RAIM does not depend on TTA, although sequential algorithms do. As of now, a TTA value for road tolling has not been set.

The integrity risk depends on the final application requirements, i.e. the invoice accuracy. If estimated positions are assumed to be supported by correct, up to date integrity information at every epoch, each faulty position not alerted contributes to the integrity risk budget:

$$P_{\text{int}} = \text{p}(X_{failure} \,|\, \text{no alert}) \tag{2}$$

C. Definition of RAIM parameters

RAIM performs two functions at each epoch:

1) it checks the availability of the fault detection function calculating the **Horizontal Protection Level (HPL)**
2) if it is available, it detects the position failure with the **Fault Detection (FD)** algorithm.

The HPL is defined as the radius of a circle with its center at the true position that describes the region where it is assured to contain the estimated horizontal position within the missed alert (P_{MA}) and false alert (P_{FA}) requirements [6]. The HPL is a function of the satellite-user geometry and of the expected pseudorange error, but not of the current measurements, so it is predictable. The HPL is compared with the HAL to decide whether the integrity function is available within the required performance (Figure 3):

- HPL<HAL: integrity function available.
- HPL>HAL: integrity function not available.

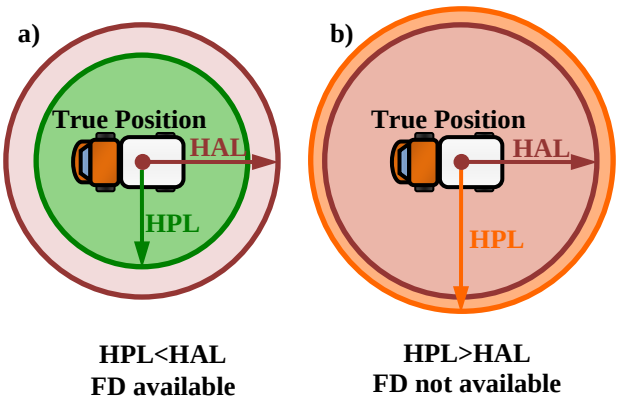

Figure 3. Upper view of a truck with examples of RAIM availability. a) HPL<HAL, b) HPL>HAL.

RAIM may also have fault exclusion (FDE) capabilities, for what FDE availability has to be checked with the Horizontal Exclusion Level (HEL).

FD detects and FDE also isolates and excludes the presence of an unacceptable large position error (position failure) using redundant measurements. Its performance is characterized by the probability of certain events of the detection and exclusion processes [6]:

- Probability of **missed detection** (P_{MD}). A missed detection occurs when a positioning failure is not detected.
- Probability of **wrong exclusion** (P_{WE}). A wrong exclusion occurs when a positioning failure exists and is firstly detected, but it still exists and is not detected after the exclusion phase.
- Probability of **missed alert** (P_{MA}). A missed alert occurs whenever a positioning failure is not warned with an alert. It can be caused by missed detection or by wrong exclusion: $P_{MA} = P_{MD} + P_{WE}$.
- Probability of **false detection** (P_{FD}). A false detection is defined as the detection of a positioning failure when a positioning failure has not occurred.
- Probability of **false alert** (P_{FA}). A false alert is defined as the indication of an alert when a position failure has not occurred. It is caused by a false detection followed by no exclusion.

Assuming FD, or FDE with probabilities of wrong exclusion and exclusion after false detection negligible, we can consider the following equivalences:

$$P_{MD} = P_{MA} \tag{3}$$
$$P_{FD} = P_{FA} \tag{4}$$

Most of the RAIM algorithms have been designed to deal with single failures. In comparison with the minimum number of satellites needed for positioning, RAIM needs to track one additional satellite to obtain the necessary redundancy to detect a failure, and two to exclude it.

D. Studies needed to design RAIM algorithms

The design of a RAIM algorithm needs two parameters, P_{MA} and P_{FA}.

The probability of missed alert is directly related with the integrity risk and the probability of position failure:

$$P_{\text{int}} = P_{position\ \ failure} \cdot P_{MA} \tag{5}$$

In order to characterize position failures, two GNSS operation modes are distinguished: nominal and faulty:

$$P_{position\ \ failure} = \quad (6)$$
$$= \left(1 - P_{faulty\ mode}\right) \cdot P_{positioning\ failure} \Big|_{\text{nominal mode}} +$$
$$+ P_{faulty\ mode} \cdot P_{positioning\ failure} \Big|_{\text{faulty mode}}$$

The nominal mode considers the position errors when all GNSS segments are working according to their specifications and the magnitude of other external error sources is within its typical values. In this case, certain user-satellite geometries may amplify the ranging error and generate a position failure. The errors are characterized by the **pseudorange nominal measurement model**.

The faulty mode includes error sources not considered in the nominal mode, like pseudorange biases due to satellite failures. The faulty mode is described by a **threat model** with information like the probability and magnitude of pseudorange biases.

The probability of false alarm will contribute to the RUC system unavailability, mainly caused by the RAIM unavailability, which in turn depends on the HPL. The HPL is a function of the RAIM, the satellite geometry and the expected error (nominal measurement model). Since there is not RAIM developed yet in this work, only unavailability caused by lack of visible satellites can be analyzed as a preliminary result.

To sum up, the following studies are required:
- Calculation of GNSS integrity requirements
  - integrity risk
- Analysis of unavailability
  - satellite visibility
- Characterization of the position failure:
  - pseudorange nominal measurement model
  - threat model

4. RUC INTEGRITY REQUIREMENTS

A RUC invoice may be erroneous because of two reasons:
- Overcharging, which consists in charging a vehicle for geo-objects (road segments) that has not used.
- Undercharging, which consists in not charging a vehicle for geo-objects that actually has used.

Both events result in unfair invoices, causing excessively high bills in the case of overcharging and loss of revenue in the case of undercharging. The aim of RUC integrity requirements is to limit the impact of over- and undercharging into known bounds. These integrity requirements may be given at three levels:

1) Requirements at service level. It is the highest level, directly related with the performance of the service provided by the application. For instance, it may define the accuracy of the final invoice, of the total distance travelled by the user, etc.
2) Requirements at geo-object level. They state the false and missed detection of the user inside a pricing segment (geo-object false/missed recognition rates)
3) Requirements on GNSS navigation level, that is, the signal-in-space integrity risk and HAL.

The three levels are interrelated, specifying the requirements in one level already sets them in the other two. The first level represents the final performance of the system directly seen by the user and the service provider. The requirements on GNSS navigation level are needed to design the RAIM algorithm, and the requirements at geo-object level are the intermediate step between the GNSS and the service levels.

A. Requirements at service level: invoice accuracy

From the point of view of the user and the service provider, the system reliability can be expressed in terms of invoice accuracy. If the invoice seems to be incorrectly high, the user may raise a complaint. Service providers can control the expected number of complaints due to overcharging and the loss of revenue due to undercharging setting the appropriate invoice accuracy. Therefore, RUC requirements at application level are likely to be specified as the invoice accuracy. For instance, in the Dutch ABvM "*the requirement set for the registration unit is that the amount, corresponding to the distances recorded over a one-month period, may not deviate by more than 1% from a 'perfect' measurement in 99% of cases*" [4]. Ref. [8] specifies that the measurement device "*should be certified to provide distance measurement accurate to within 2%*". These requirements may detail the maximum allowable rates of under- and overcharging.

B. Requirements at geo-object level

RUC performance requirements may be expressed in the maximum allowable geo-object false and missed recognition rates. So does the report of the Expert Group 9 [8] supporting the European Commission on the work of the Directive 2004/52/EC on electronic road toll systems (ref. [1]), stating that "*it is necessary to define a specific set of test conditions in which test geo-objects are guaranteed to be successfully recognized with a success rate of at least 99.99 %. False recognition of a geo-object should be less than 1 in* 10^6 ".

B.1. Relation between geo-object requirements and invoice accuracy

The invoice quantity is the accumulated charge of each segment in which the user has been detected along the invoice period. The relation between the invoice and geo-object levels depends on several parameters like number

of segments per invoice, length (price) of the segments, etc.

The probability to have n missed recognized geo-objects ($P_{n\,MR\,GO}$) in an invoice follows a binomial distribution that depends on the total number N of geo-objects the user has circulated through:

$$P_{n\,MR\,GO} = \binom{N}{n} {P_{MR}}^{n} \left(1 - P_{MR}\right)^{N-n} \tag{7}$$

Equivalently, the probability to have n false recognized geo-objects ($P_{n\,FR\,GO}$) in an invoice follows a binomial distribution that depends on the total number N of geo-objects the user has not circulated through but are candidates to suffer false recognition:

$$P_{n\,FR\,GO} = \binom{N}{n} {P_{FR}}^{n} \left(1 - P_{FR}\right)^{N-n} \tag{8}$$

These two formulas can be expressed in a general form:

$$P_{n\,EGO} = \binom{N}{n} {P_{GO\,error}}^{n} \left(1 - P_{GO\,error}\right)^{N-n} \tag{9}$$

where the probability of n erroneous geo-objects $P_{n\,EGO}$ can be $P_{n\,MR\,GO}$ or $P_{n\,FR\,GO}$, and the geo-object error rate $P_{GO\,error}$ is P_{MR} or P_{FR}.

Let's calculate the relation between $P_{GO\,error}$ and the application level requirements (maximum allowable error of x% in X% of the invoices), assuming that:

- each segment has the same price and $P_{GO\,error}$.
- an invoice contains only missed or false recognized geo-objects, but not both failure types. It is a worst case scenario because missed recognitions do not compensate the false ones and vice versa.

The maximum number of erroneous (missed or false recognized) geo-objects ($n_{\max}$) that still meets the maximum invoice error requirement (x%) is a function of N:

$$n_{\max} = 0 \text{ for } 1 \le N < \left\lceil \frac{100}{x} \right\rceil \tag{10}$$

$$n_{\max} = k \text{ for } \left\lceil k \cdot \frac{100}{x} \right\rceil \le N < \left\lceil (k+1) \cdot \frac{100}{x} \right\rceil, \text{ with } k = 1,2,3,...$$

The probability an invoice will be within the accuracy requirement is:

$$\frac{X}{100} = p\left(n \le n_{\max}\right) = \sum_{n=0}^{n_{\max}} P_{n\,EGO} \tag{11}$$

Let's assume the geo-object error probability is at least lower than the required accuracy, i.e. $P_{GO\,error} \le x/100$. In this case, the smallest X given the value of $P_{GO\,error}$ occurs with $n_{\max} = 0$ and $N = \lceil 100/x \rceil - 1$. For instance, the most demanding case to achieve a maximum error of 1% when $P_{GO\,error} \le 0.01$ consists on getting zero erroneous geo-objects in an invoice of $N = 99$. Equation (11) yields the following relation in the worst case scenario:

$$P_{GO\,error} = 1 - \left(\frac{X}{100}\right)^{\left\lceil 100/x \right\rceil - 1} \tag{12}$$

Table 1 contains the maximum allowable $P_{GO\,error}$ obtained with eq.(12) for different invoice requirements. For example, to achieve the $X = 99$% of the invoices with an undercharging below $x = 1$%, a missed recognized geo-object requirement of $P_{MR} = 10^{-4}$ is needed. The table can be seen from an overcharging point of view. For instance, to achieve a not overcharging rate of $X = 99.9$% with a vehicle that travels close to $N = 999$ geo-objects that are candidates to be overcharged, a probability of $P_{FR} = 10^{-6}$ is needed.

Table 1. Required $P_{GO\,error}$ for different requirements of invoice accuracy.

		max error (x)		
		N geo-objects		
		1 %	**0.1 %**	**0.01 %**
		99	**999**	**9999**
X	**99 %**	1e-4	1e-5	1e-6
	99.9 %	1e-5	1e-6	1e-7
	99.99 %	1e-6	1e-7	1e-8

It is important to remember that the values of Table 1 correspond to the most demanding cases; a different N would result in less restrictive P_{MR} and P_{FR} for the same invoice requirements.

C. Requirements at GNSS navigation level

The design of a RAIM algorithm needs the GNSS navigation integrity requirements, i.e. P_{int} and HAL. This section will address the calculation of P_{int} from the geo-object requirements.

The decision of the user's presence in a toll section, also known as geo-object recognition, is based on user's GNSS estimated positions that have HPL<HAL and are not detected as position failure by the FD. A small percentage of the selected positions are **hazardous misleading information (HMI)**, defined as estimated positions with

HPL<HAL but actually have an error (ε_H) larger than the maximum allowed (HAL):

$$\left.\begin{array}{c} HPL < HAL \\ \& \\ \varepsilon_H > HAL \end{array}\right\} \Rightarrow HMI \qquad (13)$$

The probability of occurrence of HMI (p_{HMI}) is caused in part by the GNSS integrity risk.

A HMI only has negative consequences on the system's liability when the user's real and estimated positions are in different sides of the geo-object. Overcharging MI occurs when the vehicle is outside the toll segment but its estimated position inside, undercharching MI consists on the opposite case (Figure 4). The worst scenario is chosen for this paper, in which every HMI has a negative impact in the geo-object recognition, which gives conservative HMI requirements. Over- and undercharging HMI are assumed to occur with the same probability:

$$p_{HMI} = p_{over\,HMI} = p_{under\,HMI} \qquad (14)$$

The process of a geo-object recognition is triggered when there is at least one estimated position inside it. First, all the GNSS positions related with the geo-object are collected and used afterwards to decide whether the vehicle has circulated through the segment or not. The set of GNSS positions can be collected taking all the positions calculated during the interval of time between the first and last estimated positions inside the toll segment. Nevertheless, some estimated positions out of the segment that should be included in the recognition process may not be selected with this method.

Let's consider the recognition of a geo-object with a set of N_{pos} estimated positions with HPL<HAL, where N_{in} are inside the segment and N_{out} outside it:

$$N_{pos} = N_{in} + N_{out} \qquad (15)$$

The position samples are assumed to be independent. Applying the maximum likelihood estimation to the geo-object recognition, the user is assumed to have been inside the segment if:

$$p\left(N_{in} | user\ inside\ geo-object\right) > p\left(N_{in} | user\ outside\ geo-object\right) \qquad (16)$$

$$\binom{N}{N_{in}} \left(1-p_{MI}\right)^{N_{in}} p_{MI}^{\,N-N_{in}} > \binom{N}{N_{out}} \left(1-p_{MI}\right)^{N_{out}} p_{MI}^{\,N-N_{out}}$$

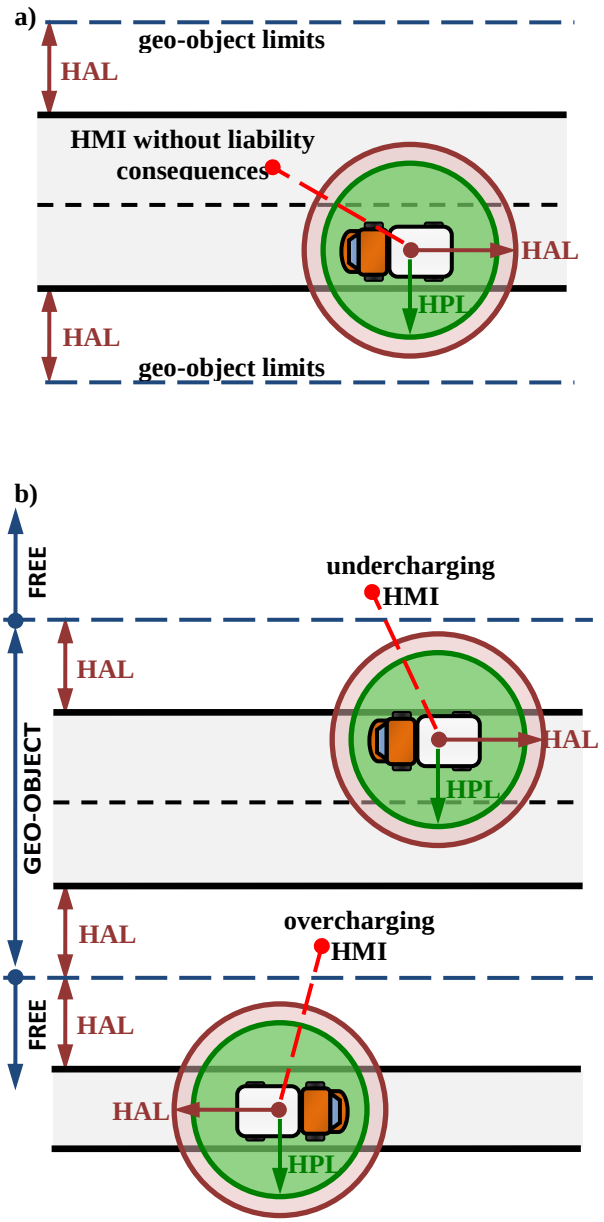

Figure 4. Examples of a) HMI without liability consequences, b) over- and undercharging HMI.

Solving eq.(16) for $p_{MI} << 1$, the maximum likelihood estimation is equivalent to the majority voting method:

$$N_{in} > N_{out} \Rightarrow \text{user inside geo} - \text{object} \qquad (17)$$

In the case of equality we give priority to avoid overcharging rather than undercharging:

$$N_{in} \leq N_{out} \Rightarrow \text{user outside geo} - \text{object} \qquad (18)$$

C.1. Relation between the probability of missed/false recognized geo-object and the probability of MI

The probability of geo-object false recognition is a function of the available number of position samples (N_{pos}) and the HMI probability (Figure 5):

$$p_{FR} = p\left(N_{in} > N_{out} \middle| \text{user outside geo} - \text{object}\right) = \quad (19)$$
$$= \sum_{n=\lfloor N_{pos}/2 \rfloor + 1}^{N_{pos}} \binom{N_{pos}}{n} \cdot {p_{HMI}}^{n} \cdot \left(1 - p_{HMI}\right)^{N_{pos}-n}$$

If only one independent position sample is available, GNSS MI directly causes segment false recognition and $p_{MI} = p_{FR}$. A higher N_{pos} loosens up the HMI requirements. For instance, a $p_{FR} = 10^{-6}$ is reached with a p_{MI} of $6 \cdot 10^{-4}$ when the decision is taken with 2 or 3 independent position samples. The necessary p_{MI} decreases to $4 \cdot 10^{-3}$ when there are 4 or 5 available samples and to 10^{-2} with 6 or 7.

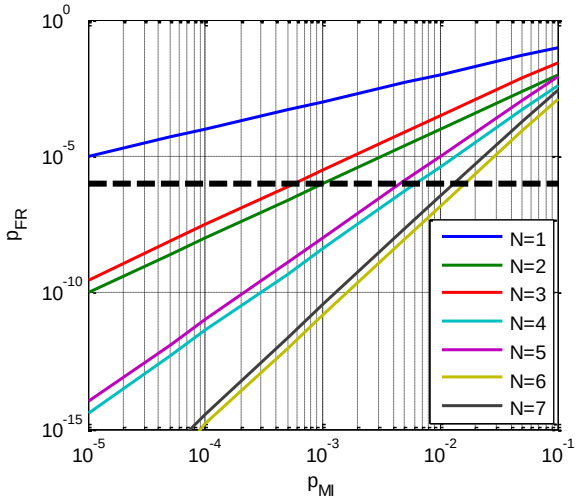

Figure 5. Relation between the probability of GNSS MI p_{MI} and the probability of false recognized geo-object p_{FR} for various number of independent position samples.

Geo-object missed recognition may be caused by 1) unavailability of the system (absence of estimated positions within the integrity requirements) or 2) by undercharging MI.

$$p_{MR} = p_{MR/unavailability} + p_{MR/MI} \quad (20)$$

The geo-object missed recognition probability due to MI is (Figure 6):

$$p_{MR/MI} = p\left(N_{in} \le N_{out} \middle| \textit{user inside geo} - \textit{object}\right) = \quad (21)$$
$$= \sum_{n=\lceil N_{pos}/2 \rceil}^{N_{pos}} \binom{N_{pos}}{n} \cdot {p_{HMI}}^{n} \cdot \left(1 - p_{HMI}\right)^{N_{pos}-n}$$

A GNSS MI directly causes a missed segment when there are only one or two independent position samples, giving in that case $p_{MI} \approx p_{MR/MI}$. As an example, let's consider that there are more samples and set the same HMI probability as in the false recognition case with two or three samples, $p_{MI} = 6 \cdot 10^{-4}$. This gives $p_{MR/MI} = 2 \cdot 10^{-6}$ and $p_{MR/unavailability} = 9.8 \cdot 10^{-5}$.

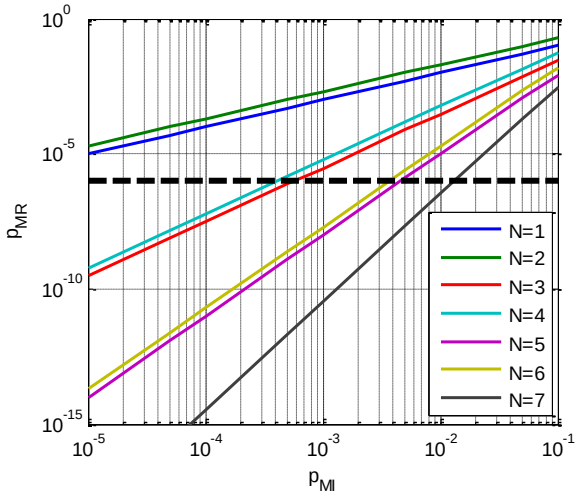

Figure 6. Relation between the probability of GNSS MI (p_{MI}) and the probability of missed recognition of a geo-object (p_{MR}) for various number of independent position samples.

The number of independent samples has an important effect in the required MI probability, the higher the better. As will be explained in one of the next sections, positions of single-frequency receivers are likely to be correlated along the geo-object because of the long correlation time of the residual ionospheric delay, which usually reduces the number of independent position samples per geo-object to one. On the other hand, dual frequency receivers may perform segment recognition with several independent samples.

C.2. Relation between p_{MI} and p_{int}

Finally, the HMI risk is distributed in the different system blocks that contribute to its generation in order to obtain the GNSS integrity risk. The quantity allocated at each block indicates the maximum allowed HMI probability for that block. Following the example of p_{HMI} of $6 \cdot 10^{-4}$ the GNSS integrity risk results $p_{\text{int}} = 1.5 \cdot 10^{-4}$.

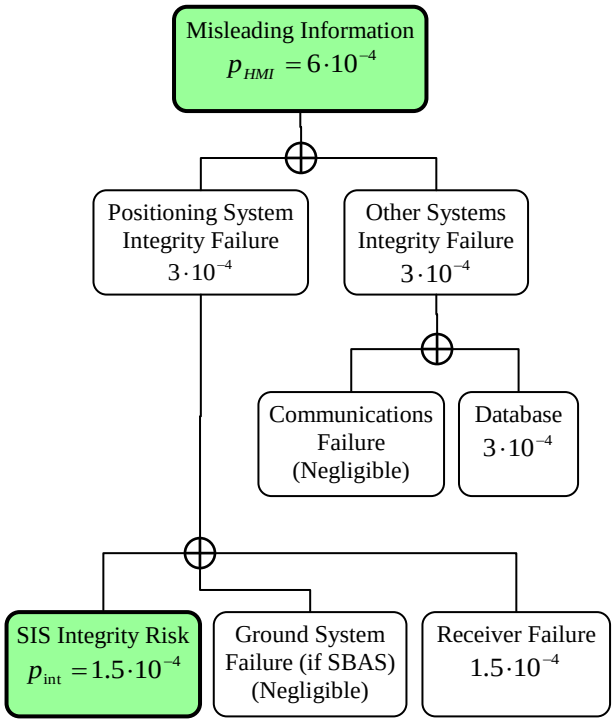

Figure 7. Distribution of the MI risk. Probabilities are given per independent sample.

5. GNSS VISIBILITY

Urban environments have an important number of obstacles that block the visibility of GNSS satellites. A reduced number of satellites not only causes RUC unavailability, but also degrades the in-view satellite geometry and consequently the system's performance. This section analyzes the effect of GNSS visibility on the capability of using RAIM.

Bi-dimensional navigation requires a minimum of three satellites; RAIM needs one additional satellite for detecting one faulty ranging source and two for excluding it. Let's consider a detection-only RAIM and a single faulty satellite; in this case, the RAIM can be used when the number of satellites is equal or higher than four.

Figure 8 and Figure 9 show the PDF of the length of the periods with less and more than 4 visible satellites in a urban environment. Only satellites with LOS are considered available. Data have been obtained with a 24-hour simulation in a 2°-step user position grid located in Europe [34°N-72°N, 9°E-43°W]. The number of satellites of the GNSS constellation is 24 for GPS and 27 for Galileo; satellite positions have been calculated from almanacs. The simulated urban scenario is similar to that used for the multipath model: a vehicle circulating at 50 km/h along the axis of a 20-meter wide street with buildings at both sides of the road and an average height of 15 meters. The number of visible satellites have been computed every second for various azimuth angles of the street axis.

The duration of periods with less than 4 satellites is typically less than 10 seconds. The worst case, which occurs with a very low probability, is 135 seconds for standalone GPS and 25 seconds for bi-constellation GPS/Galileo receivers. Because the transit time in a toll segment is usually longer, it is assured that the RAIM will be ready to be used several times per segment. Nevertheless, this fact only assures the capacity of the RAIM to compute the HPL, but not its availability, which requires HPL<HAL. Further simulations with the RAIM are needed to obtain its availability.

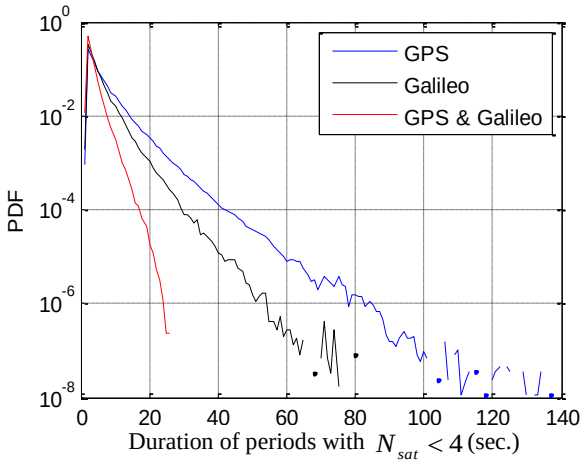

Figure 8. Length of periods with less than 4 visible satellites.

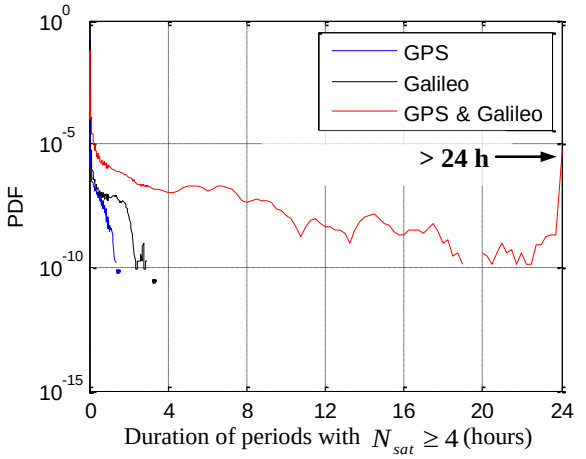

Figure 9. Length of periods with more than 4 visible satellites.

6. NOMINAL PSEUDORANGE MEASUREMENT MODEL

The model describes the pseudorange measurement error distribution a road user can expect in a urban scenario at nominal conditions, that is, with the errors due to any GNSS segment within their specifications and the magnitude of other external error sources within its typical values. A deeper explanation of the model can be found in [9]. Errors resulting from failure of any GNSS segment are excluded from this model. The receiver may be single- or dual-frequency and use GPS, Galileo, both of them or SBAS augmentation.

Pseudorange measurement errors are modeled by zero-mean Gaussian distributions characterized by their variance $\varepsilon_{PSR} \sim N(0, \sigma_{PSR})$. Conservative models obtained with overbounding techniques are used in order to include all possible errors, counting as well those of large magnitude and low probability.

The PSR measurement error is assumed to be the result of five independent error sources: thermal noise and interferences, ionospheric delay, tropospheric delay, inaccuracies in the broadcast ephemeris and satellite corrections, and multipath. Each individual error source is also modeled as a zero-mean gaussian distribution, so the variance of the total pseudorange measurement error is the addition of the variance of each error source:

$$\sigma^2_{PSR} = \sigma^2_{noise} + \sigma^2_{iono} + \sigma^2_{tropo} + \sigma^2_{clock\&ephem} + \sigma^2_{multipath} \quad (22)$$

A. Thermal noise and interferences

The code tracking error due to thermal noise at the receiver's front-end input is a function of the signal modulation and the receiver design. For a Dot-Product discriminator its variance is given by [10]:

$$\sigma^2_{DP} = \frac{B_L\left(1 - 0.5 \cdot B_L T_I\right) \int_{-B/2}^{B/2} G_s(f) \sin^2(\pi f d) \cdot df}{\frac{C_s}{N_0}\left(\int_{-B/2}^{B/2} 2\pi \cdot f \cdot G_s(f) \sin(\pi f d) \cdot df \right)^2} \cdot \left(1 + \frac{1}{\frac{C_s}{N_0} T_I \int_{-B/2}^{B/2} G_s(f) df} \right) \quad (23)$$

The effect of interferences can be simulated with the thermal noise error obtained by setting the C/No as the PLL loss-of-lock threshold.

B. Satellite's clock and ephemeris equivalent range error

Inaccuracies on the SV clock corrections and ephemeris broadcast in the navigation message cause range errors whose magnitude depends on the GNSS used. The error model is directly broadcast in the navigation message.

Galileo broadcast the SISA (Signal in Space Accuracy), which is the predicted minimum standard deviation of the overbounding error distribution. A nominal SISA of 0.85 meters is taken, which is the maximum allowable value to meet the Galileo RAMS (Reliability, Availability, Maintainability, and Safety) requirements [11].

GPS transmits the URA (User Range Accuracy), defined as the standard deviation of the error. Its nominal value is currently 3.9 meters [12], but this value is expected to decrease as the system evolves. In this work we assume a nominal URA of 0.85 meters in modernized GPS, which is the same value of the nominal SISA for Galileo (the definitions of URA and SISA are however different).

SBAS provides satellite clock and ephemeris corrections, as well as its residual overbounding error model, which standard deviation is mainly defined by the UDRE (User Differential Range Error). A nominal UDRE of 0.3 meters has been obtained with an EGNOS simulator, which is assumed to be representative of other SBAS.

$$\sigma_{clock\&ephemeris} = \begin{cases} 3.9\,m, & current\ GPS \\ 0.85\,m, & future\ GPS \\ 0.85\,m, & Galileo \\ 0.3\,m, & SBAS \end{cases} \quad (24)$$

C. Ionospheric delay

Four ionospheric correction types are considered in this paper: dual frequency, GPS, Galileo and SBAS. Each correction method yields a different residual error.

C.1. Dual frequency

Dual-frequency pseudorange combinations remove the first order model of the ionospheric delay, independently of the GNSS employed (GPS or Galileo). Remaining errors due to higher order effects are typically negligible:

$$\sigma_{iono,\ dual\ frequency} \cong 0 \quad (25)$$

The drawback of dual frequency iono-free measurements is that the pseudorange combination amplifies the error components that are different at each frequency, that is, thermal noise, interferences and multipath.

C.2. GPS

The coefficients α and β broadcast by GPS allow to estimate the ionospheric delay at the user's zenith ($T_{iono,\ vert}$) as a function of time and the receiver position following the model described in [13]. The result is afterwards scaled by the obliquity factor (F) to obtain the final correction:

$$T_{iono} = F \cdot T_{iono,\ vert} \quad (26)$$

where:

$$F = 1 + 16 \cdot \left(0.53 - \frac{E}{180} \right)^3 \quad (27)$$

In general, GPS corrections are able to correct 50 % of the ionospheric delay. A more detailed overbounding residual error model for GPS L1 civil aviation receivers is defined in [6]. The fact that the model is used in a SoL application like civil confirms its reliability. For this reason, the

residual error model considered in this paper is based in the civil aviation one. In order to simplify the expression, the obliquity factor of eq.(27) is used:

$$\sigma_{iono,GPS} = F \cdot \max\left\{0.2 \cdot c \cdot T_{iono,vert}, \tau_{vert}\right\} \quad m \tag{28}$$

where VTEC is the Vertical Total Electron Content and F is the obliquity factor defined in (27). This residual error model has been assessed and validated in [14].

C.2. Galileo

The nominal $\sigma_{iono,Galileo}$ is obtained as the minimum value obtained with a given percentile of the International GNSS Service (IGS) VTEC database [15]. The adequate percentile of needs to be chosen according to the integrity requirements of the application.

Figure 10 compares the GPS and Galileo ionospheric residual error models proposed in this section. Note that they have been obtained differently: the GPS model is the one used in civil aviation, the Galileo one has been obtained from a VTEC database of the last 12 years.

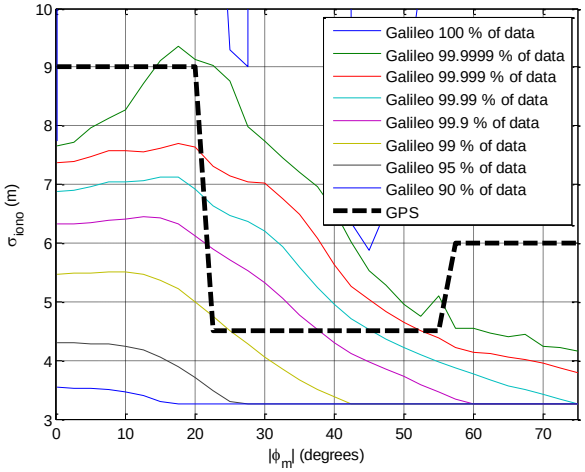

Figure 10. Galileo and GPS ionospheric residual error model

C.3. SBAS

SBAS broadcast a regional grid of ionospheric corrections and the standard deviation of its residual error at the zenith, GIVE (Grid Ionospheric Vertical Error). A nominal GIVE of 0.46 meters has been calculated with an EGNOS simulator, which is assumed to be representative of other SBAS. Afterwards, the GIVEs around the user's position are interpolated to obtain the UIVE (User Ionospheric Vertical Error). The nominal UIVE is also 0.46 meters. Finally, the nominal error model is the UIVE scaled by the obliquity factor of eq.(27):

$$\sigma_{iono,SBAS} = F \cdot 0.46 \quad m \tag{29}$$

D. Tropospheric delay

Tropospheric delay are caused by local phenomena. As a consequence, no corrections are broadcast by any GNSS, including SBAS. It is the user instead who directly calculates them with a model stored in the receiver. Consequently, the residual error depends on the correction model applied by the user and not on the GNSS employed. In this work we select the same correction algorithm as in civil aviation, described in Appendix A of [6]. As in the ionospheric delay case, the fact that the model has been selected for a SoL application like civil aviation is a proof of its reliability. Its residual error only depends on the satellite elevation angle:

$$\sigma_{tropo} = 0.12 \cdot m(E) \cdot \sigma_{TVE} \quad m \tag{30}$$

where:

$$m(E) = \frac{1.001}{\sqrt{0.002001 + \sin^2 E}} \cdot \left(1 + 0.015 \cdot \left(\max[0, 4° - E]\right)^2\right) \quad \text{for } E > 2°$$

E. Multipath

Multipath, especially important in urban scenarios, depends on the user's local environment. As a consequence, it cannot be corrected by parameters broadcast by any GNSS or SBAS and it is the user itself that should be provided with a model to bound the possible error due to multipath. This section proposes such a model of multipath error for road users in urban environments calculated via Monte Carlo simulations with a channel and a receiver simulators.

First, time series of multipath data, i.e. amplitude (A), phase (θ) and delay (τ) of direct and reflected rays, are calculated with a channel model designed for vehicular GNSS users in urban environments [16]. The simulation scenario consists on a user circulating at 50 km/h along the axis of a 20 meter wide road, with the antenna at 1.5 meters of height. The buildings, at both sides of the street, have an average height of 15 meters. The output sampling frequency is 1 kHz, which meets for user speeds up to 90 km/h the value of 8/λ recommended for urban channels. The data has been computed at different azimuth (0°, 90°) and elevation (0°, 90°) angles with steps of 10°. Simulations have been performed for L1 and they are assumed to be representative of the multipath behavior at other frequencies.

Secondly, the output of the channel model is processed by a receiver simulator to obtain the pseudorange error. The correlator outputs are the result of the contribution of each multipath ray. For instance, the in-phase prompt output is:

$$I_P = \sum_{i=1}^{N} A_i \cdot \tilde{K}_c\left(\varepsilon_\tau + \Delta\tau_i\right) \cdot \cos\left(\varepsilon_\theta + \Delta\theta_i\right) \tag{31}$$

- N is the total number of LOS and multipath rays

- $\tilde{\tilde{K}}_c$ is the filtered PRN code autocorrelation function
- C_s is the Early-Late spacing (chips)
- $\varepsilon_\tau = \tau_1 - \hat{\tau}$, is the DLL synchronization error with regard to the LOS ray
- $\Delta\tau_i = \tau_i - \tau_1$, is the delay of the i^{th} ray with regard to the LOS ray
- $\varepsilon_\theta = \theta_1 - \hat{\theta}$, is the PLL synchronization error with regard to the LOS ray
- $\Delta\theta_i = \theta_i - \theta_1$ is the phase difference of the i^{th} ray with regard to the LOS ray

The receiver simulator employs the autocorrelation function (K_c) of a whole PRN sequence, thus the minimum sampling period of the correlator output is the PRN sequence length. Nevertheless, the correlator model also assumes the signal parameters (A, θ, τ) remain constant during the calculation of each output, but their required sampling period is 1 ms, which is shorter than certain PRN codes. It has been proven during the study that any 1-ms segment of any PRN sequence has autocorrelation characteristics comparable to those of the current L1 C/A code. The receiver model is therefore valid for PRN longer than the period time of 1 ms.

Thirdly, the correlator output is accumulated with an integration period (T_I) of 20 ms. Afterwards, a lock detector based on PLL and C/N_0 estimators selects the samples that will employ the user. Since the real delay of the signal is known from the channel model, the computation of the pseudorange error of each sample is straightforward.

It is important to notice that the receiver is assumed to work properly and not to introduce additional errors. The simulated receiver configurations are commonly used in civil aviation, that is, integrity based applications. The receiver has lost track of most of the signals affected with long multipath biases due to the large phase change commonly associated to the apparition of long biases. In addition, the lock detector output is verified by an algorithm that removes isolated large errors. As a consequence, the multipath error can still be modeled as a zero-mean Gaussian function.

Finally, the obtained error database is modeled with an overbounding zero-mean normal distribution following the CDF overbounding technique [17]. The multipath error model has been obtained as a function of the satellite elevation angle (Figure 11).

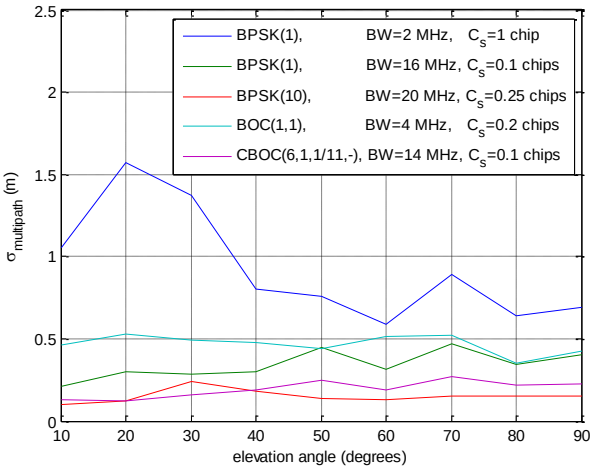

Figure 11. Final multipath overbounding error model (T_I=20 ms, Lock detector average period = 500 ms)

F. *Final PSR error model*

The final error model is calculated with eq. (22). For example, Figs.14-16 plot the results for different GNSS signals, a receiver with a DP discriminator and a coherent integration time of 20 ms, C/N_0 of 40 dBHz, the user at a geomagnetic latitude of 50° and the equivalent error due to the SV clock and ephemeris inaccuracies set to the one corresponding to modernized systems (URA=SISA=0.85 m)

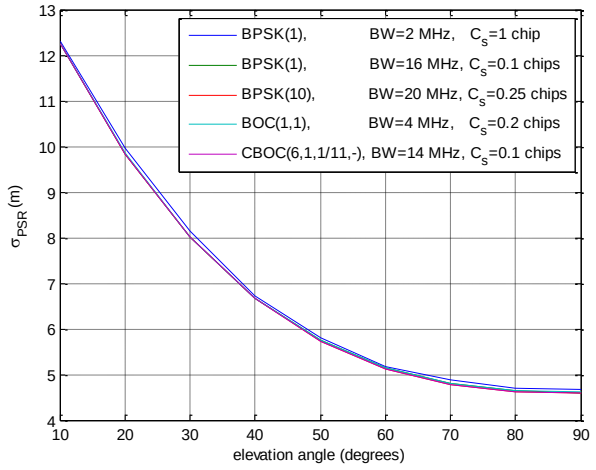

Figure 12. Pseudorange nominal measurement model. Single frequency receiver with GPS ionospheric corrections.

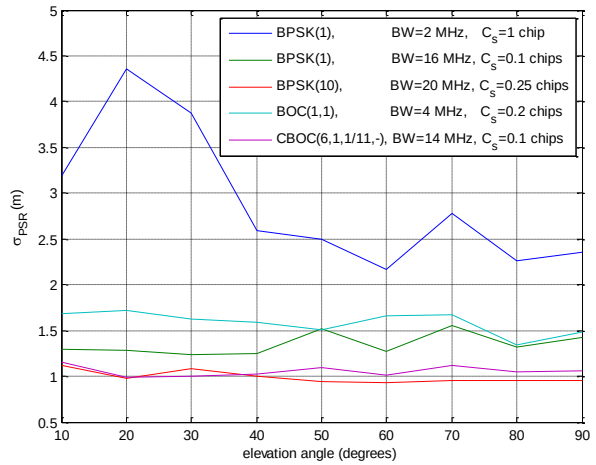

Figure 13. Pseudorange nominal measurement model. Dual frequency receiver.

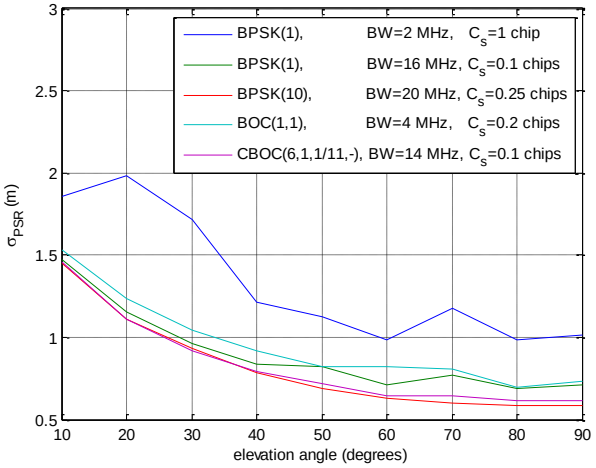

Figure 14. Pseudorange nominal measurement model. Single frequency receiver with SBAS ionospheric, SV clock and ephemeris corrections.

7. CORRELATION OF ESTIMATED POSITIONS

The relations between probability of false/missed segment recognition and of GNSS MI of eqs.(19) and (21) depend on the number of uncorrelated position samples. This section analyzes the correlation time of the error of the estimated positions.

The correlation time of the position error depends on the characteristics of the pseudorange measurements used in the estimation, which are derived from the error sources identified in the nominal measurement model. Except for the thermal noise and multipath, the error correlation time defined in civil aviation in [6] are taken. Pseudorange error sources are modeled as a first order Markov process with the following correlation times:

- Ionospheric residual errors: the model follows the International Ionosphere Reference 2001. Typical correlation values are around 30 minutes.
- Tropospheric residual errors: 30-minute correlation time, which is representative of a typical storm passing by.
- Satellite clock and ephemeris errors: 2-hour correlation time.
- Thermal noise and multipath errors: a correlation time around 1 second has been obtained during the simulations to obtain the multipath contribution to the nominal measurement model. Additionally, a DLL bandwidth of 1 Hz indicates a thermal noise correlation close to 1 second. Thus, a correlation time of a few seconds is taken.

The pseudorange correlation time is a function of the magnitude and correlation of each error source. In general, ionospheric errors, thermal noise and multipath are the largest error sources and dominate the final correlation time. Pseudorange errors in non-SBAS single frequency receivers are driven by the ionospheric one, resulting in a correlation time close to 30 minutes. On the other hand, dual-frequency receivers present an error correlation of a few seconds, mainly driven by the thermal noise and multipath. The dominant error source in SBAS single frequency receivers depends on the GNSS signal robustness against noise and multipath.

The position error depends on the satellite geometry. Then, the error correlation changes with the number of satellites and their geometry. The longest correlation time corresponds to the scenario when the same satellites are used during the whole pseudorange correlation time. In that case, the correlation period of the position error can be as long as the pseudorange one.

It can be concluded that the correlation time will be longer in single-frequency receivers than in dual frequency ones because of the effect of the ionospheric delay. Then, it is more probable that single frequency receivers will perform segment recognition with only one independent position sample, which results in the equivalency between position failure and erroneous geo-object recognition. Dual frequency receivers are more likely to provide several independent position estimations per road segment, which improves the performance of the geo-object recognition.

8. THREAT MODEL: CRITICAL BIAS

The threat model considers the errors not included in the nominal mode, such as bias due to satellite failures.

The position error in nominal conditions follows a bidimensional Gaussian distribution which is the result of the satellite geometry and the Gaussian distribution of each pseudorange measurement error. The equiprobable error magnitude is described by an ellipse. In the presence of a bias, this ellipse is displaced towards the HAL limits, incrementing the position failure probability. This section characterizes the minimum bias that leads to a position failure.

This work considers biases caused by satellite major failures. A GPS major failure is defined as an error larger than 4.42 times the URA. The GPS signal specification states that 3 major failures per year are allowed in the whole satellite constellation:

$$p_{individual\ \ major\ failure} = 1.25 \cdot 10^{-5} / h \qquad (32)$$

The same satellite failure probability will be used for Galileo. The probability of multiple satellite failure is assumed to be negligible. The critical bias can be obtained numerically as explained in [18].

An example of the critical biases obtained at a given instant with a 24 GPS and 27 Galileo satellite constellation is shown in Figs. 15 and 16. The data has been obtained in a worldwide grid of user positions in order to obtain a variety of satellite geometries, with a HAL of 50 meters, a standard deviation of the nominal error of 1 meter and two different mask angles, 5° and 15°.

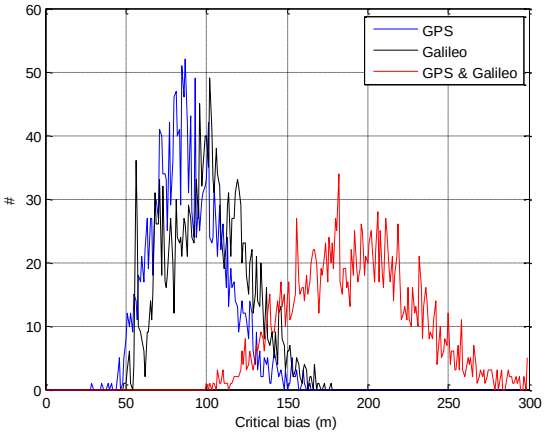

Figure 15. Critical bias histogram (HAL=50 m, $P_{\text{int}} = 10^{-4}$, $\sigma_{PSR} = 1$ m, $P_{sat\ failure} = 1.25 \cdot 10^{-5}$, mask angle = 5°).

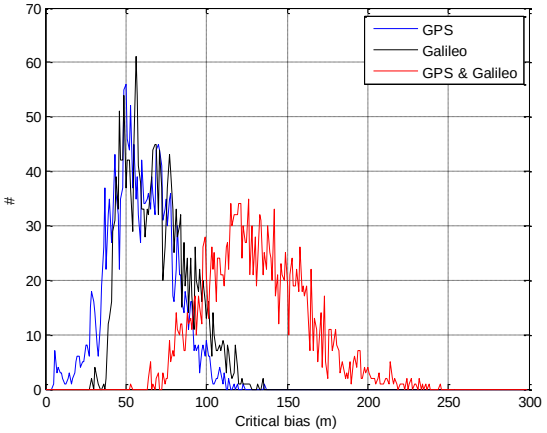

Figure 16. Critical bias histogram (HAL=50 m, $P_{\text{int}} = 10^{-4}$, $\sigma_{PSR} = 1$ m, $P_{sat\ failure} = 1.25 \cdot 10^{-5}$, mask angle = 15°).

The minimum critical bias obtained with a mask angle of 5° is large enough to be considered a major failure, so they can be characterized by the probability of eq.(32). Higher mask angles degrade the in-view satellite geometry, reducing the size of the critical bias. For instance, with a mask angle of 15° the minimum critical bias for standalone GPS presents low values that may not be caused only by major failures.

To sum up, the critical bias is the minimum bias that the RAIM should be able to detect. It depends on the integrity risk, the HAL and the satellite geometry, so it has to be calculated for each environment and set of integrity requirements. Further analysis have to be carried out in order to fully characterize the critical bias in conditions of degraded visibility.

CONCLUSIONS AND FUTURE WORK

The paper has presented previous studies needed to develop RAIM algorithms for road tolling applications in urban environments.

First, the role of geo-fencing and geo-object recognition has been explained, showing the importance of the segment length. Afterwards, several concepts of GNSS integrity necessary to understand RAIM techniques have been introduced, and the three main analysis necessary to design RAIM algorithms have been identified as the characterization of the integrity requirements, the system unavailability and the position failures. Concerning the integrity requirements, the formulas that relate the application needs and the GNSS integrity risk have been calculated and examples have been provided. The effect of the correlation time of position errors has been highlighted, reasoning that single frequency receivers are likely to have poorer segment recognition performance due to the large correlation time of the ionospheric delay. The study of satellite visibility in urban environment has provided satisfactory results for the use of RAIM, but further analysis including the HPL computation must be carried out to obtain its final availability. The position errors have been characterized in the nominal and faulty conditions. A pseudorange nominal measurement model has been computed for road users in urban environments with several receiver configurations. The threat model for satellite major failures has been introduced, although further studies are required for scenarios of degraded visibility.

The future work includes the complete determination the threat model in urban environments, the design of the FD and HPL algorithms and the final evaluation of the RAIM performances.

REFERENCES

[1] European Parliament and the Council of the European Union, "on the interoperability of electronic road toll systems in the Community", Official Journal of the European Union, 29 April 2004

[2] Toll Collect, "Truck Toll in Germany. User Information", Edition 2009.
[3] NDSAS (Motorways and Express roads in Slovakia), "Multi-lane Free-flow Electronic Tolling in the Slovak Republic", February 2010
[4] "Explanatory memorandum of the Dutch Road Pricing Act", English version, available in the website of the Dutch Ministry of Transport, Public Works and Water Management
[5] Ministry of Ecology, Energy, Sustainable development and Regional development of France, "Partnership contract concerning the national HGV eco-tax and the Alsace experimental tax. Project presentation note", March 31, 2009 (English version November 2, 2009)
[6] Radio Technical Commission for Aeronautics (RTCA), "Minimum Operational Performance Standards (MOPS) for Global Positioning System (GPS)/ Wide Area Augmentation System (WAAS) Airborne Equipment", RTCA DO-229D, December 2006
[7] International Civil Aviation Organization (ICAO), "International Standards and Recommended Practices. Annex 10, Aeronautical Telecommunications. Volume I, Radio Navigation Aids" Sixth edition, July 2006
[8] Expert Group 9, "Report of Expert Group 9 Working to support the European Commission on the work on Directive 2004/52/EC: Specification of the EFC application based on satellite technologies", version 3.2, 20 February 2006
[9] D. Salós, C. Macabiau, A. Martineau, B. Bonhoure, D. Kubrak, "Nominal GNSS Pseudorange Measurement Model for Vehicular Urban Applications", IEEE/ION PLANS, 3-6 May 2010.
[10] Julien O., "Design of Galileo L1F tracking loops", PhD thesis, University of Calgary, Department of Geomatics Engineering, 2005
[11] V. Oehler, F. Luongo, J.P. Boyero, R. Stanford, H.L. Trautenberg, J. Krueger, J. Hahn, F. Amarillo, M. Crisci, B. Schlarmann, J.F. Flamand, "The Galileo Integrity Concept", ION GNSS 2004
[12] D. Have, "Reference set of parameters for RAIM availability simulations", working paper Sofreavia, 8-9 April, 2003
[13] B. Arbesser-Ratsburg, "The Galileo Single Frequency Ionospheric Corection Algorithm", Third European Space Weather Week, 13-17 November, 2006
[14] N.C. Rogers, J.E.N. Field, C. Griffin, P.S. Cannon, M.J. Angling, M. Hollreiser, "An assessment of the Galileo single frequency correction model", Second European Space Weather Week, 14 - 18 November 2005
[15] Hernandez-Pajares, M. Hernández-Pajares, J. M. Juan, J. Sanz, R. Orus, A. Garcia-Rigo, J. Feltens, A. Komjathy, S. C. Schaer, A. Krankowski, "The IGS VTEC maps: a reliable source of ionospheric information since 1998", Journal of Geodesy, 2009, Volume 83, pp. 263-275
[16] A. Lehner, A. Steingass, "A Novel Channel Model for Land Mobile Satellite Naviagtion", ION GNSS 18th International Technical Meeting of the Satellite Division, 13-16 Sept. 2005
[17] B. DeCleene, "Defining Pseudorange Integrity - Overbounding", ION GPS 2000, 19-22 September 2000
[18] A. Martineau, "Performance of Receiver Autonomous Integrity Monitoring (RAIM) for Vertically Guided Approaches", PhD thesis, Institute National Polytechnique de Toulouse, 2008